IEEE Access
Multidisciplinary ⋮ Rapid Review ⋮ Open Access Journal

Received 21 December 2022, accepted 3 January 2023, date of publication 25 January 2023, date of current version 1 February 2023.

Digital Object Identifier 10.1109/ACCESS.2023.3239591

RESEARCH ARTICLE

Robust and Optimal Control Designed for Autonomous Surface Vessel Prototypes

MURILLO FERREIRA DOS SANTOS[1], ACCACIO FERREIRA DOS SANTOS NETO[1], LEONARDO DE MELLO HONÓRIO[2], MATHAUS FERREIRA DA SILVA[2], AND PAOLO MERCORELLI[3], (Member, IEEE)

[1]Department of Electroelectronics, CEFET-MG, Leopoldina 30421-169, Brazil
[2]Department of Energy Systems, UFJF, Juiz de Fora 36036-900, Brazil
[3]Institute for Production Technology and Systems (IPTS), Leuphana University of Lüneburg, Lüneburg, 21335 Lower Saxony, Germany

Corresponding author: Paolo Mercorelli (paolo.mercorelli@leuphana.de)

This work was supported in part by the German Research Foundation (DFG); in part by the Open Access Publication Fund of Leuphana University of Lüneburg; in part by the Federal University of Juiz de Fora, Brazil; in part by the Santo Antônio Energia, under the supervision of the Brazilian Regulatory Agency of Electricity (ANEEL), under Project PD-06683-0122/2022; in part by Centro Federal de Educação Tecnológica de Minas Gerais (CEFET-MG); in part DAAD; and in part by the Leuphana University of Lüneburg.

ABSTRACT It is well known that activities in running water or wind and waves expose the Autonomous Surface Vessels (ASVs) to considerable challenges. Under these conditions, it is essential to develop a robust control system that can meet the requirements and ensure the safe and accurate execution of missions. In this context, this paper presents a new topology for controller design based on a combination of the Successive Loop Closure (SLC) method and optimal control. This topology enables the design of robust autopilots based on the Proportional-Integral-Derivative (PID) controller. The controllers are tuned from the solution of the optimal control problem, which aims to minimize the effects of model uncertainties. To verify the effectiveness of the proposed controller, a numerical case study of a natural ASV with 3 Degree of Freedom (DoF) is investigated. The results show that the methodology enabled the tuning of a PID controller capable of dealing with different parametric uncertainties, demonstrating robustness and applicability for different prototype scenarios.

INDEX TERMS Robust control design, successive loop closure, optimal control, PID controller, autonomous surface vehicles.

I. INTRODUCTION

Among autonomous vehicles, Autonomous Surface Vessels (ASVs) are the ones that increasingly attract researchers around the world. Characterized by low cost, high mobility, and a high degree of autonomy, these vehicles offer applications in a wide variety of marine environments [1], [2], [3]. It is possible to find applications in lakes, rivers and open seas. Activities can range from water and harbor monitoring [4], shallow water hydrological survey [5], maritime search and rescue [6], bathymetric mapping [7], and many other applications [8].

Given the great diversity of environments and activities, ASVs are subject to scenarios from calm waters to environments with high exposure to disturbances (for example, currents, winds, and waves) [9], [10]. Furthermore, vessels can also be exposed to challenging applications in shallow waters such as swamps, estuaries, mangroves, lagoons, and coral reefs [11], [12]. In these conditions, conventional vessels cannot operate easily due to limitations imposed on maneuverability and care taken to ensure that the propellers are not damaged. These aspects lead to the need of developing ASVs with a greater maneuverability from new propulsion system topologies and control adjustment techniques [13].

Besides, under difficult operating conditions, the unmodeled dynamics can not be covered by the control system, which can arise and compromise the safety and reliability of the operations. Therefore, it also promotes the need for robust control systems in challenging and uncertain scenarios.

The associate editor coordinating the review of this manuscript and approving it for publication was Ton Duc Do.

However, designing robust control systems is not a trivial task. A control system is considered robust only when it can guarantee robust stability and/or performance in the presence of assumed uncertainties (e.g., parametric variations, neglected nonlinearities, and unmodeled dynamics) [14], [15]. To reach these criteria, it is necessary to deal with complex solution spaces, convergence problems for specific uncertain sets, and difficulties in obtaining sufficiently robust and simple models to develop control techniques [16]. Moreover, there is also a consensus on the need to seek simplicity in design and practical implementation.

A. STATE OF THE ART AND RELATED WORKS

A quick search on the internet shows many and different ASV topologies for different applications.

In spite of these innovative ASVs, there are still situations that those approaches could need improvements or a better performance. At this moment, let's consider the contributions [13] and [17], where an over-actuated catamaran ASV was designed for shallow waters: it is still necessary to implement well-tuned controllers to perform missions as they are requested.

Taking the methodology for controller tuning, many control approaches have been found in the literature to deal with the mentioned problem. Conventional PID controller, High-Gain State Observer (HGSO), adaptive control, Sliding-Mode Control (SMC), intelligent control, and H-infinity technique are some approaches [18].

Within the scope of PID controllers, the works [19], [20], [21] are examples of successful applications in ASVs. Although these approaches have their limitations when dealing with highly coupled nonlinearities and time-varying dynamics, they are often preferred due to their synthesis and simplification [22]. To reduce these initial limitations, several studies have been conducted to overcome them by combining other techniques, such as in paper [23].

Papers [24], [25], [26] present applications of HGSO in marine vehicle control. It is possible to understand from these works the benefits of applying a well-designed HGSO that makes the control system robust to system uncertainties and with high disturbance rejection. Furthermore, the works also demonstrate the success in obtaining the stability proof of the closed-loop system. It can be an obstacle for systems with complex models and make the applied methodology hard in some cases.

Classical adaptive control approaches are found in the contributions [27], [28], [29]. Specifically, work [27] depicts a comparative study between the techniques of gain scheduling, model reference adaptive control, and L_1 adaptive control. Both methods are investigated in the speed control of the SeaFox vessel, seeking to minimize the effects of the propulsion system uncertainties that occur between low and high-speed operating modes. Good results are observed even in transition and high-speed modes. It is also clear that such techniques must be applied carefully, especially in situations of great uncertainty. Under these conditions, in particular, the convergence problems and parametric oscillations can run, impairing the desired stability and robust performance.

Related to methodologies based on SMC, works [30], [31], [32] are interesting examples of application in ASVs. Paper [31] presents a classic SMC application, while [30] and [32] show changes to increase the closed-loop system robustness and reduce control system chattering. Regardless of the approach adopted, all the contributions were devoted to the initial objectives and are satisfactory in the presence of disturbances and parametric uncertainties. However, it is also possible to understand that the SMC must be applied more carefully, as the controlling action of the rigid slip mode can lead to chattering, energy loss, plant damage, and unmodeled dynamic excitation.

In artificial intelligence approaches, it is possible to find applications of artificial neural networks, Bayesian probability, fuzzy logic, machine learning, evolutionary computation, genetic algorithms, or a combination of these methods. Works [18], [33], [34] present some of these applications. Although intelligent controllers have proven to be good control options, typically, this approach requires a long parameter-setting process. They are often used in experimental vehicles, although industrial vehicles are still an opportunity for these control techniques [35].

Finally, regarding robust control techniques, the papers [36], [37] are interesting examples. Both articles propose controllers based on the infinite control theory that could deal with the uncertainties involved. However, it is noteworthy that the approaches provide strong robustness, also requiring complex solution processes, which deserve attention in establishing the problem [38].

Through the mentioned work, it is possible to understand the difficulties in designing a robust controller. A key element in this process is the simplicity of the control topology. Simpler control laws make testing and implementation steps easier. Therefore, avoiding control law synthesis requires sophisticated numerical solution methods and time-consuming hardware implementation [39]. In this sense, the development of robust controllers based on the traditional PID is a promising path, as long as it is combined with other techniques that overcome the deficiencies of the PID controller [23].

In this direction, the combination of the SLC method with optimal control is quite innovative. To the authors' knowledge, there are no robust PID controller tuning algorithms with these characteristics applied to ASVs. A fact that can be explored and later applied to vehicle driving in general, such as the control algorithms developed in [40] and [41].

B. CONTRIBUTIONS

This work is a part of a project where some important publications were previously done, which are:

- Citation number [13]: Hull and Aerial Holonomic Propulsion System Design for Optimal Underwater Sensor Positioning in Autonomous Surface Vessels;

- Citation number [17]: Project and Control Allocation of a 3 DoF Autonomous Surface Vessel With Aerial Azimuth Propulsion System;
- Citation number [42]: Development of Optimal Parameter Estimation Methodologies Applied to a 3DoF Autonomous Surface Vessel.

The first one is focused on the ASV design, looking at its construction to minimize the effects and interference of its displacements in the water on the Acoustic Doppler Current Profiler (ADCP) sensor, embedded in the ASV. The second one takes the ASV design and control allocation into account, using also the traditional laws for its modeling. The third one looks at the ASV parameters identification, where a new methodology for optimal parameter estimation was applied and proved. Both of these 3 works were experimentally tested.

Under this background, this paper presents a new control design topology from the combination of the Successive Loop Closure (SLC) method and optimal control. This topology allows the designing of robust autopilots based on PID controllers. The controllers are adjusted from the solution of the optimal control problem using the Interior-Point Algorithm (IPA) to minimize the effects of model uncertainties. A numerical case study of a real ASV with 3 DoFs investigates the proposed controller effectiveness, exposing it to uncertainty scenarios based on the vessel's operational movements.

After this summary, the main contributions of this paper can be written below, and thus:

- Depicts the modeling and identification of a catamaran type ASVs with aerial propulsion, considering the coupled hydrodynamics parameters, which are not well explored in the literature;
- Presents a robust controller tuning methodology based on SLC and optimal control to design PID autopilots in cascade control applied to an ASV;
- Makes in-depth a case study about controller tuning of real ASV in solution space $\mathbb{R}^{12}$ and robust stability analysis of closed-loop control with uncertainty analysis in $\mathbb{R}^{27}$.

C. PAPER ORGANIZATION

This paper is organized as follows: Section II presents the robust control problem, showing its characteristics and complexities; Section III deals with the vessel used for the study and development of the robust control technique; Section IV describes the new methodology of robust control; Section V presents the numerical results of the application of the method in different scenarios; and Section VI presents some concluding remarks.

II. PROBLEM STATEMENT

Assuming that the Nonlinear Dynamic Systems (NDS) is satisfactorily approximated by a nonlinear parametric model $\mathcal{M}(\boldsymbol{\Theta})$, Equation 1 is presented:

$$\mathcal{M}(\boldsymbol{\Theta}) = \begin{cases} \dot{\boldsymbol{x}}(t) = \boldsymbol{f}(\boldsymbol{x}(t), \boldsymbol{u}(t, \boldsymbol{\Gamma}), \boldsymbol{\Theta}(t)) \\ \boldsymbol{y}(t) = \boldsymbol{h}(\boldsymbol{x}(t), \boldsymbol{u}(t, \boldsymbol{\Gamma}), \boldsymbol{\Theta}(t)), \end{cases} \tag{1}$$

where $\boldsymbol{f}$ and $\boldsymbol{h}$ are the nonlinear functions of the system, $\boldsymbol{x} \in \mathbb{R}^n$ is the state vector, $\boldsymbol{u} \in \mathbb{R}^p$ is the action vector of the PID controller, $\boldsymbol{y} \in \mathbb{R}^m$ is the output vector, $\boldsymbol{\Theta} \in \mathbb{R}^r$ is set of uncertain parameters about NDS and $\boldsymbol{\Gamma} \in \mathbb{R}^q$ represents the PID controller parameters.

Suppose that $\boldsymbol{\Theta}$ is unknown, time-variant and contains an uncertainty region $\boldsymbol{\Omega} \in \mathbb{R}^r$. Also, $\boldsymbol{\Omega}$ is a region around the *priori* estimate $\hat{\boldsymbol{\Theta}}$ with radius $\boldsymbol{\delta\Theta}$. Therefore, $\boldsymbol{\Theta}$ is defined by:

$$\boldsymbol{\Theta}(t) = \hat{\boldsymbol{\Theta}} + \boldsymbol{\delta\Theta}(t). \tag{2}$$

In this context, the design problem of a robust PID controller can be defined as: "find the control law parameters $\boldsymbol{u}(t, \boldsymbol{\Gamma})$ such as the closed-loop system is globally asymptotically stable and has robust performance for all the parametric uncertainty region $\boldsymbol{\Omega}$".

The optimal control can also fulfill the controller robustness, establishing an optimization problem whose minimization assures the robustness criteria. In this way, the controller design can be expressed by the following optimization problem:

$$\mathcal{S}(\mathcal{M}(\hat{\Theta} + \delta\Theta), \Gamma^-, \boldsymbol{\mathcal{X}}) = \Gamma^+, \tag{3}$$

where $\boldsymbol{\Gamma}^-$ is the vector of the PID controller initial parameters, $\boldsymbol{\mathcal{X}}$ is the established reference vector to the controller loops, and $\mathcal{S}$ is an arbitrary nonlinear optimization algorithm that searches for the best $\boldsymbol{\Gamma}^{\oplus} \in \mathbb{R}^q$. Finally, the posterior parameter set obtained by $\mathcal{S}$ is defined by $\boldsymbol{\Gamma}^+$.

III. THE AUTONOMOUS SURFACE VESSEL PROTOTYPE

The ASV is a vessel developed to autonomously collect hydrological measurements in environments with underwater obstacles, and shallow and fast water flows.

Based on a catamaran-type vessel, this ASV has an innovative air propulsion system with azimuth control. This setting generates an ASV with 3 over-actuated DoFs, highly maneuverable and capable of operating in the situations mentioned above. Fig. 1 shows the vessel developed. More information about it is found in works [13], [17].

For the best presentation of the ASV coordinate frames, Fig. 2 is shown:
where roll, pitch and yaw angles (ϕ, θ, ψ) are measured in the Inertial Frame $\mathcal{F}^I$ $(\hat{i}^I, \hat{j}^I, \hat{k}^I)$ which considers the Vehicle Frame $\mathcal{F}^v$ (translation transformation from $\mathcal{F}^I$) and the Body-Fixed Frame $\mathcal{F}^b$ $(\hat{i}^b, \hat{j}^b, \hat{k}^b)$.

A. MODELING AND IDENTIFICATION

Traditional surface vessel modeling requires its development from the description of 3 DoFs, i.e., x and y axis translation movements (*Surge* and *Sway*) and rotation around the z-axis

FIGURE 1. Real view of ASV.

(*Yaw*). The others DoFs are disregarded due to their small influence over the vessel's dynamics [43].

According to the marine vehicle nomenclature, the state vectors are expressed as follows: $\boldsymbol{\eta} = [x, y, \psi]^T$ representing inertial (x, y) and angular (ψ) positions in the vehicle inertial frame $\mathcal{F}^I$; $\boldsymbol{\nu} = [u, \upsilon, r]^T$ representing the linear (u, v) and angular (r) velocities in the Rigid-Body frame $\mathcal{F}^b$ [43].

The general ASV dynamics and kinematics modeling (without disturbance) is represented as follows [44]:

$$M\dot{\boldsymbol{\nu}} + C(\nu)\nu + D(\nu)\nu = \boldsymbol{\tau}, \tag{4}$$

$$\dot{\boldsymbol{\eta}} = \boldsymbol{J}(\psi)\boldsymbol{\nu}, \tag{5}$$

where $\boldsymbol{M} \in \mathbb{R}^{3\times3}$ is the Inertia Matrix; $\boldsymbol{C}(\boldsymbol{\nu}) \in \mathbb{R}^{3\times3}$ is the Coriolis and centripetal Matrix; $\boldsymbol{J}(\psi)$ is the Jacobian matrix that relates the velocities in the Rigid-Body and the inertial frame; $\boldsymbol{D}(\boldsymbol{\nu}) \in \mathbb{R}^{3\times3}$ is the hydrodynamic damping; $\boldsymbol{\tau} \in \mathbb{R}^{3\times1}$ is the vector of generalized forces and moments applied by the propellant system.

Considering all the couplings between 3 DoFs, the matrices $\boldsymbol{M}, \boldsymbol{C}(\boldsymbol{\nu})$ and $\boldsymbol{J}(\psi)$ are presented as [44]:

$$\boldsymbol{M} = \begin{bmatrix} m - X_{\dot{u}} & -X_{\dot{v}} & -X_{\dot{r}} \\ -Y_{\dot{u}} & -Y_{\dot{v}} & mx_g - Y_{\dot{r}} \\ -N_{\dot{u}} & mx_g - N_{\dot{v}} & I_z - N_{\dot{r}} \end{bmatrix}, \tag{6}$$

$$\boldsymbol{C}(\boldsymbol{\nu}) = \begin{bmatrix} 0 & 0 & -\beta_2 \\ 0 & 0 & \beta_1 \\ \beta_2 & -\beta_1 & 0 \end{bmatrix}, \tag{7}$$

$$\boldsymbol{J}(\psi) = \begin{bmatrix} \cos(\psi) & -\sin(\psi) & 0 \\ \sin(\psi) & \cos(\psi) & 0 \\ 0 & 0 & 1 \end{bmatrix}, \tag{8}$$

where m is the vehicle total mass, I_z is the z-axis moment of inertia, x_g is the gravity center displacements on x-axis. Additionally, the elements $X_{\dot{u}}, X_{\dot{v}}, X_{\dot{r}}, Y_{\dot{u}}, Y_{\dot{v}}, Y_{\dot{r}}, N_{\dot{u}}, N_{\dot{v}}, N_{\dot{r}}$ represent the hydrodynamic derivatives of the added mass phenomenon. Moreover, $\beta_1 = mu + [X_{\dot{u}}u + X_{\dot{v}}v + X_{\dot{r}}r]$ and $\beta_2 = -m(x_g r + v) + [Y_{\dot{u}}u + Y_{\dot{v}}v + Y_{\dot{r}}r]$.

Finally, the hydrodynamic damping $\boldsymbol{D}(\boldsymbol{\nu})$ is expressed by the superposition of linear and nonlinear damping, and this is associated with quadratic damping. Thus, $\boldsymbol{D}(\boldsymbol{\nu})$ is expressed by [44]:

$$\boldsymbol{D}(\boldsymbol{\nu}) = \begin{bmatrix} -X_u & -X_v & -X_r \\ -Y_u & -Y_v & -Y_r \\ -N_u & -N_v & -N_r \end{bmatrix} + \begin{bmatrix} -X_{|u|u}|u| & -X_{|u|v}|u| & -X_{|u|r}|u| \\ -Y_{|v|u}|v| & -Y_{|v|v}|v| & -Y_{|v|r}|v| \\ -N_{|r|u}|r| & -N_{|r|v}|r| & -N_{|r|r}|r| \end{bmatrix}, \tag{9}$$

where the elements $X_u, X_v, X_r, Y_u, Y_v, Y_r, N_r, N_u, N_r$ represent the linear damping, while all the others represent the nonlinear damping of a quadratic order.

TABLE 1. Vessel inertial parameters.

Parameter	Value	Unit
m	20.80	$[kg]$
I_z	02.98	$[kg.m^2]$
x_g	-0.05	$[m]$
y_g	0.00	$[m]$

The vessel parameters were identified in two stages. First, the inertial characteristics were obtained by direct measurements and Computer-Aided Design (CAD) tools. Later, the parameters of the $\boldsymbol{M}$, $\boldsymbol{C}(\boldsymbol{\nu})$ and $\boldsymbol{D}(\boldsymbol{\nu})$ were estimated by the rSOESGOPE method, proposed by [42]. This methodology favors robust parametric estimation, which is fundamental to the problem addressed in this work. The results are shown in Tables 1 and 2.

It is important to highlight that the parameters from the table above were validated with open-field experiments in the work [42], where this ASV was exhaustively tested in a real and non-controlled environment.

B. STRUCTURE AND CONTROL LEVELS

This section will describe the structure control developed in this work and embedded in the over-actuated ASV.

This vehicle performs maneuvers using differential torque on the motors or tilting their 4 servomotors independently. This type of possibility leads this vehicle to be faster, more versatile, and have a great torque application, among other benefits. In addition, this vehicle performs yaw maneuvers just by adjusting the 4 servomotors tilting angles.

However, these abilities lead to implementing a different control allocation technique for the vehicle's actuators. This is due to the existence of 3 Virtual Control Actions (VCAs) and 8 Real Control Actions (RCAs) (4 propulsion motors and 4 servomotors), which in fact has a non-unique solution. The control allocation technique considered is named Fast Control Allocation (FCA), which was expanded from the technique presented in [45] and [46].

To overall illustrate the control loops in a simplified procedure, Fig. 3 shows the ASV overall control structure, also with the control allocation task:

Considering this figure, it is possible to see that the input parameter to set the path is only the sequence of WayPoint

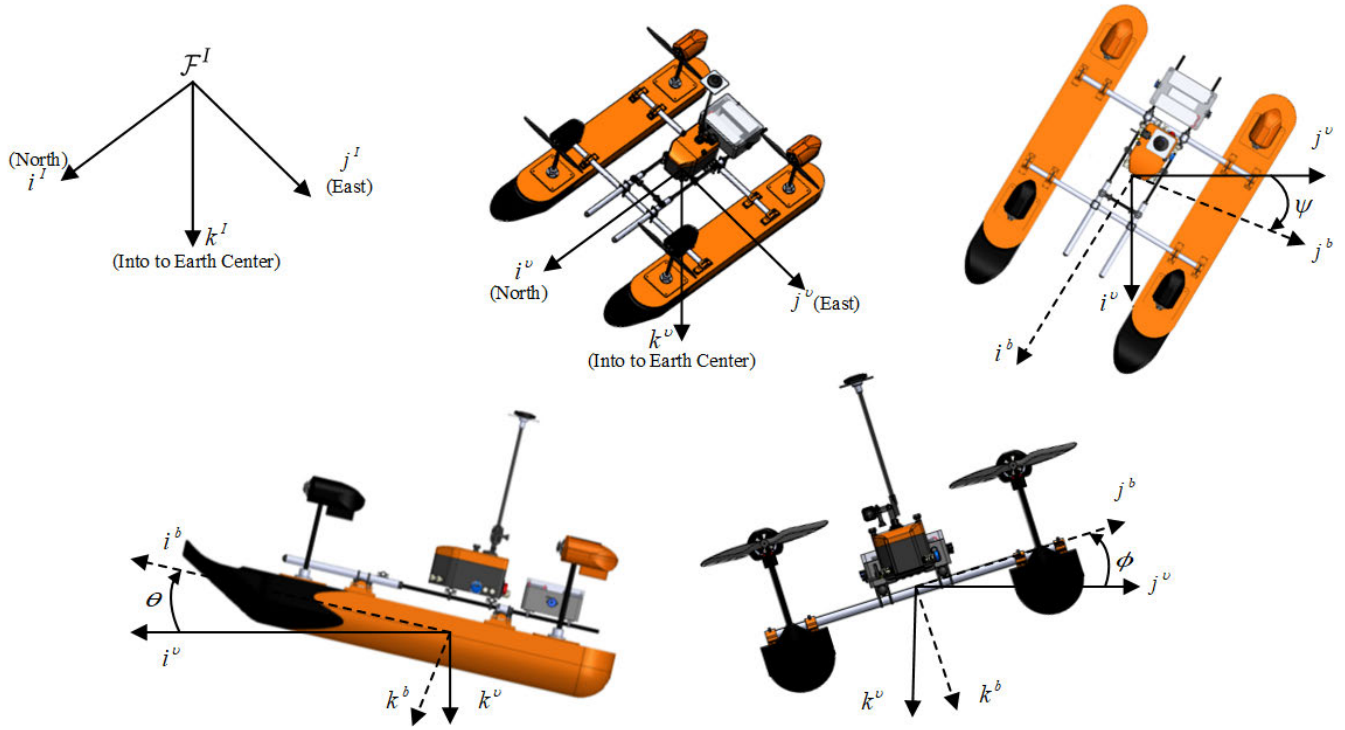

FIGURE 2. ASV coordinates frames and variables.

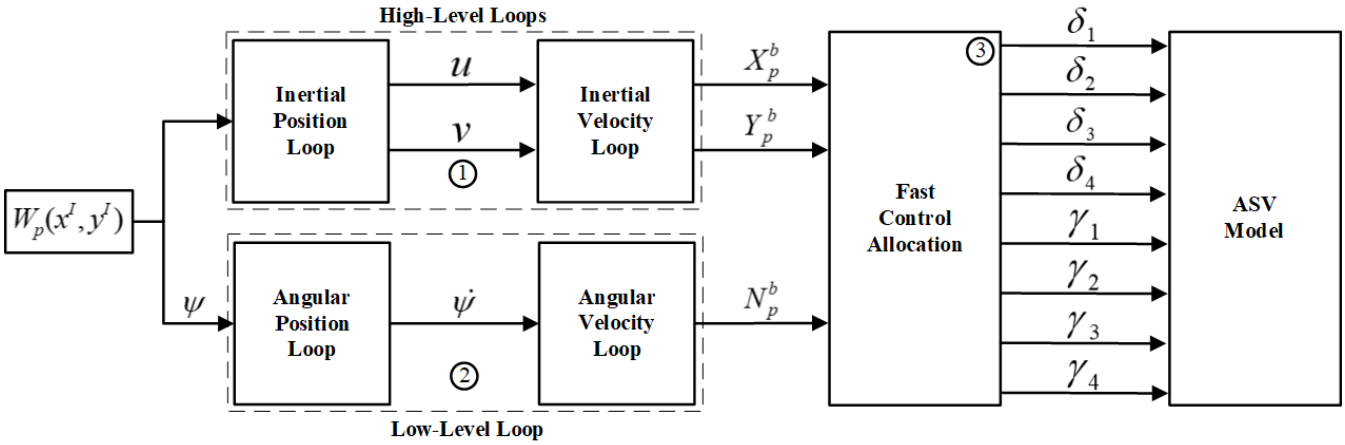

FIGURE 3. ASV overall control structure.

(WP) ($W_p(x^I, y^I)$). After that, the 3 desired setpoints are obtained inside each loop.

Then, the control loops were implemented considering two parallel levels: **High-Level Loops** (circle number 1) and **Low-Level Loops** (circle number 2). The high-level one runs at 80Hz and is responsible for controlling the inertial position loops (x^I and y^I), which deliver X_p^b and Y_P^b virtual control actions. The low-level loop runs at 400Hz and deals with the angular position loop (ψ), presenting N_p^b virtual control action.

The circle number 3 represents the control allocation technique described in Subsection III-B1.

Furthermore, every control loop level has 2 feedback cascade structures: external and internal. The outer one is a position control loop (with a Proportional (P) controller), and the inner one is a velocity control loop (with a PID controller).

The external controller is in charge of the position stability of the controlled variable through the controller P. Thus, the output control action P will be the internal control loop input PID in cascade [47]. It is essential to highlight that the output from the external loop is in the inertial referential frame, which is translated to the body-fixed frame before being used in the internal one.

In the integral loops, a saturating block was inserted, functioning as an *anti-windup* action, preventing the final control action saturation obtained only from the integral action.

To finish the control aspect information from Fig. 3, Low-Pass Filters (LPFs) were implemented to mitigate the abrupt

TABLE 2. Summary of the a priori estimation $\mathcal{M}(\Theta^{-})$.

Parameter	Value	Unit
$X_{\dot{u}}$	-17.93	$[kg]$
$X_{\dot{v}}$	0.00	$[kg]$
$X_{\dot{r}}$	0.00	$[kg \cdot m/rad]$
$Y_{\dot{u}}$	-6.67	$[kg]$
$Y_{\dot{v}}$	-19.93	$[kg]$
$Y_{\dot{r}}$	-5.37	$[kg \cdot m/rad]$
$N_{\dot{u}}$	0.00	$[kg \cdot m]$
$N_{\dot{v}}$	-5.79	$[kg \cdot m]$
$N_{\dot{r}}$	-8.49	$[kg \cdot m^2/rad]$
X_u	0.00	$[kg/s]$
X_v	-39.93	$[kg/s]$
X_r	-4.77	$[kg \cdot m/(rad \cdot s)]$
Y_u	0.00	$[kg/s]$
Y_v	0.00	$[kg/s]$
Y_r	0.00	$[kg \cdot m/(rad \cdot s)]$
N_u	-0.93	$[kg \cdot m/s]$
N_v	-6.89	$[kg \cdot m/s]$
N_r	0.00	$[kg \cdot m^2/(rad \cdot s)]$
$X_{\|u\|u}$	-7.14	$[kg/m]$
$X_{\|u\|v}$	-16.06	$[kg/m]$
$X_{\|u\|r}$	0.00	$[kg \cdot m/rad]$
$Y_{\|v\|u}$	-22.47	$[kg/m]$
$Y_{\|v\|v}$	-189.99	$[kg/m]$
$Y_{\|v\|r}$	0.00	$[kg \cdot m/rad]$
$N_{\|r\|u}$	0.00	$[kg]$
$N_{\|r\|v}$	-13.36	$[kg]$
$N_{\|r\|r}$	0.00	$[kg \cdot m^2/rad^2]$

TABLE 3. Minimum and maximum values for saturation blocks presented in Fig. 11.

Saturated Variable	Minimum	Maximum
$u^d\ [m \cdot s]$	-1.0	2.0
$v^d\ [m \cdot s]$	-1.0	1.0
$r^d\ [deg \cdot s]$	-90.0	90.0
$X_p^b\ [N \cdot m]$	-78.0	78.0
$Y_p^b\ [N \cdot m]$	-78.0	78.0
$N_p^b\ [N \cdot m]$	-42.0	42.0

derivative control actions, created to pass signals with a frequency lower than the cutoff frequency and inhibit the passage of signals with frequencies higher than this frequency (5 times slower than the cutoff frequency of the respective control loops).

To illustrate it, a block diagram of the external and internal control loops is shown in Fig. 11.

Also for this figure and the ASV's design characteristics, Table 3 presents the minimum and maximum limits used in saturation blocks:

1) FAST CONTROL ALLOCATION

The control allocation task transforms $\boldsymbol{\tau}$ VCAs (from controllers) into RCAs $\boldsymbol{u}$ driven to the system actuators. Furthermore, it is known that it may occur impossible to solve it only by matrix manipulation, instead more complex and time-consuming algorithms must be used (i. e., such as the primal-dual optimization algorithm [48]). These approaches may make the processing costs prohibitive for some onboard hardware.

Taking these remarks into account, the FCA technique proposed in [46] aims to turn the nonlinear control approach into a faster linear version by breaking the problem into two interconnected subsets of VCAs and RCAs.

The reasons for choosing these rules are:

- The nonlinearities were broken into independent problems and solved recursively and iteratively;
- The solution speed and solvability were enhanced with a subsystem coupling all the others together;
- Although this approach is not as robust as Interior-Point algorithms, it is fast and well established in the literature [49].

For the projected ASV, the VCAs are:

$$\boldsymbol{\tau} \in \mathbb{R}^3 = [X_p^b, Y_p^b, N_p^b]^T, \tag{10}$$

where N_p^b is the yawing torque, X_p^b and Y_p^b are the resultant force components on the X^b and Y^b ASV body-fixed frame, respectively.

As mentioned previously, the solution of the control allocation procedure has 8 RCAs (outputs), as presented in equations 11, 12 and 13.

$$\boldsymbol{u} \in \mathbb{R}^8 = [\boldsymbol{u_1}, \boldsymbol{u_2}]^T, \tag{11}$$

$$\boldsymbol{u_1} \in \mathbb{R}^4 = [f_1, f_2, f_3, f_4]^T, \tag{12}$$

$$\boldsymbol{u_2} \in \mathbb{R}^4 = [\gamma_1, \gamma_2, \gamma_3, \gamma_4]^T, \tag{13}$$

where f_i and γ_i are RCAs for each propulsion motor and servomotor, respectively, with $\boldsymbol{u_1}$ and $\boldsymbol{u_2}$ representing the individual propulsion signals and angles for each actuator set.

Taking these considerations into account, equation 14 is presented:

$$\hat{\boldsymbol{\tau}} = \boldsymbol{M_1}(\boldsymbol{u_2})\boldsymbol{u_1}, \tag{14}$$

where $\boldsymbol{M_1}(\boldsymbol{u_2}) \in \mathbb{R}^{3\times4}$ is the ASV Control Effectiveness Matrix (CEM), $c\gamma_i = \cos\gamma_i$ and $s\gamma_i = \sin\gamma_i$, $l_x = 0.405$ $[m]$ and $l_y = 0.375$ $[m]$ are the lever arms formed between the vehicle's center of gravity and the thrust set position.

In consequence, the propulsion motor signals are presented in equation 15:

$$\begin{bmatrix} f_1 \\ f_2 \\ f_3 \\ f_4 \end{bmatrix} = \boldsymbol{M_1^{\dagger}}(\boldsymbol{u_2}) \begin{bmatrix} X_p^b \\ Y_p^b \\ N_p^b \end{bmatrix}, \tag{15}$$

where $\boldsymbol{M_1^{\dagger}}(\boldsymbol{u_2})$ is the Moore-Penrose inverse matrix of $\boldsymbol{M_1}(\boldsymbol{u_2})$.

$$\boldsymbol{M_1}(\boldsymbol{u_2}) = \begin{bmatrix} c\gamma_1 & c\gamma_2 & c\gamma_3 & c\gamma_4 \\ s\gamma_1 & s\gamma_2 & s\gamma_3 & s\gamma_4 \\ k_1 & k_2 & k_3 & k_4 \end{bmatrix}, \tag{16}$$

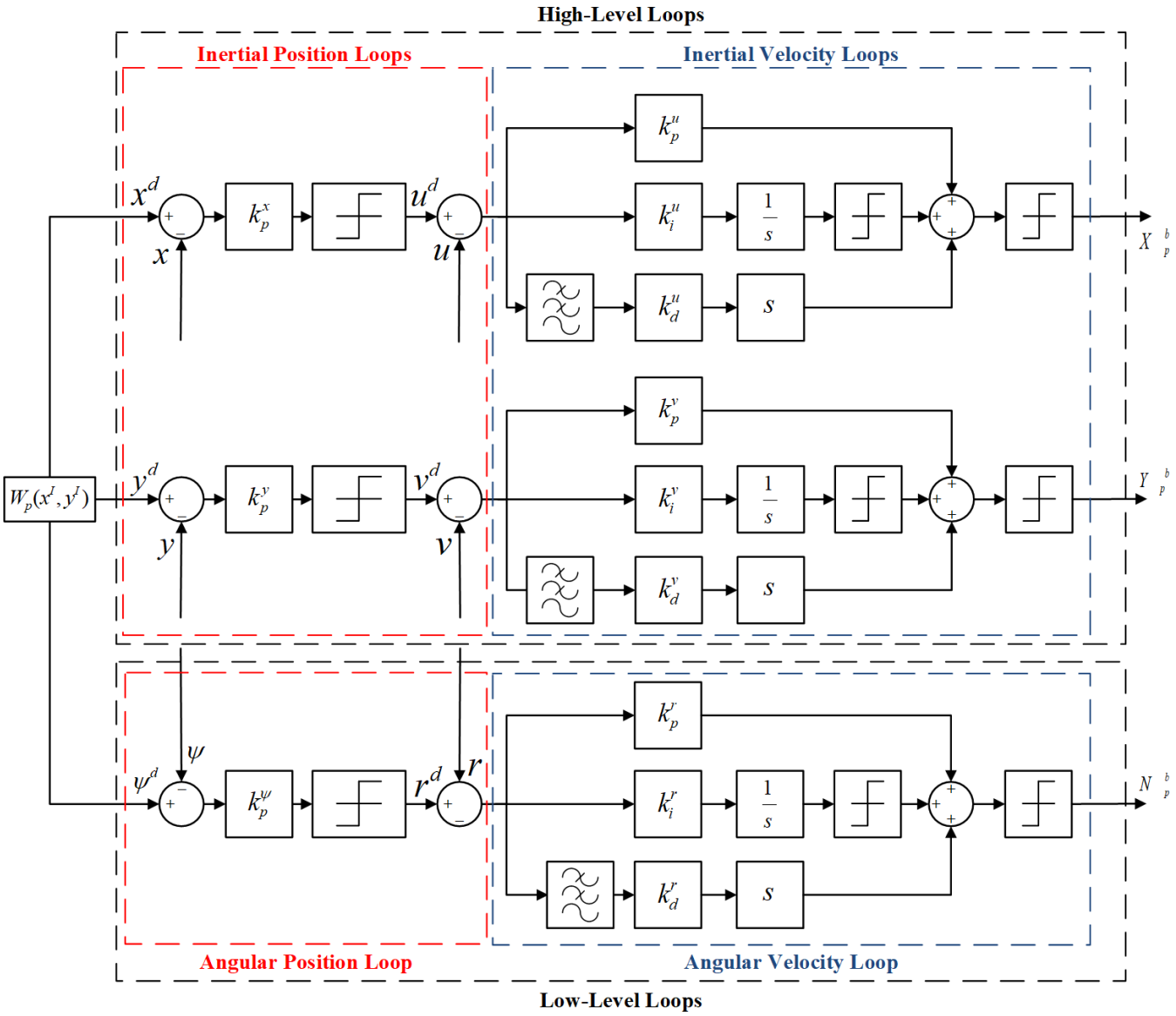

FIGURE 4. ASV position and velocity control loops.

where $k_1 = -l_y c\gamma_1 + l_x s\gamma_1$, $k_2 = l_y c\gamma_2 - l_x s\gamma_2$, $k_3 = l_y c\gamma_3 + l_x s\gamma_3$ and $k_4 = -l_y c\gamma_4 - l_x s\gamma_4$.

The servomotor tilting angles are obtained after breaking the nonlinearities, overlapping the previous solution space of $\boldsymbol{\tau}$:

$$\hat{\boldsymbol{\tau}} = \boldsymbol{M_2}(\boldsymbol{u_1})\boldsymbol{u_2}', \tag{17}$$

$$\boldsymbol{u_2}' = [c\gamma_1, s\gamma_1, c\gamma_2, s\gamma_2, c\gamma_3, s\gamma_3, c\gamma_4, s\gamma_4], \tag{18}$$

$$\boldsymbol{M_2}(\boldsymbol{u_1}) = \begin{bmatrix} f_1 & 0 & f_2 & 0 & f_3 & 0 & f_4 & 0 \\ 0 & f_1 & 0 & f_2 & 0 & f_3 & 0 & f_4 \\ -l_y & l_x & l_y & -l_x & l_y & l_x & -l_y & -l_x \\ c\gamma_1 & s\gamma_1 & 0 & 0 & 0 & 0 & 0 & 0 \\ 0 & 0 & c\gamma_2 & s\gamma_2 & 0 & 0 & 0 & 0 \\ 0 & 0 & 0 & 0 & c\gamma_3 & s\gamma_3 & 0 & 0 \\ 0 & 0 & 0 & 0 & 0 & 0 & c\gamma_4 & s\gamma_4 \end{bmatrix}. \tag{19}$$

To get the final servomotors tilting angles:

$$\boldsymbol{u_{2i}} = \text{atan2}(\sin(\gamma_i), \cos(\gamma_i)). \tag{20}$$

It is important to highlight that lines 4 to 7 from Equation 19 are mathematical constraints to enforce the property $\sin^2(\gamma_i)+\cos^2(\gamma_i) = 1$, ensuring the system does not find any sin or cos out of the trigonometric unit circle.

Then, the matrices from Equations 15 to 20 are solved interactively until the convergence criteria are reached.

C. PARAMETRIC UNCERTAINTY

Before presenting the methodology, it is worth expanding the problem related to parametric uncertainties of ASVs and the PID controller design.

Among the difficulties, the first one faced is the difficulty of modeling hydrodynamic phenomena. Since these are

highly non-linear characteristics, mathematical representation is not a trivial task [50]. Typical ASV models do not consider couplings and asymmetries, which possibly create uncertainty about the model.

Allied with the complexity of hydrodynamic phenomena, the difficulty of identifying parametric models is also a reality [1]. Usually involving complex solution spaces, the problem requires competent methodologies for excitation signal design and parameter estimation to reduce the sources of uncertainty, and coarse dynamic errors [42].

Disturbances are another undisputed sources of uncertainty, which are hardly measured and require advanced approaches for estimation [51]. It is still valid to mention sources of uncertainty such as dynamic variations in operation, mechanical changes in projects, or even inconsistencies between planned and executed projects.

Regardless of the type or source of uncertainty, it is agreed that they affect the vessel's control performance. Traditionally based on parametric models, PID controllers are very affected since the design is made from a priori parameterization subject to uncertainty. Therefore, ignoring the uncertainties in the PID control design can lead to considerable performance losses [23].

Specifically, in the problem formulated by the ASV modeling, the uncertainties are treated as structural uncertainties or resulting from parametric variations. Considering that the inertial parameters of the vessel are known variables, then the problem lies in the uncertainties about the hydrodynamic derivatives of $\boldsymbol{M}, \boldsymbol{C}(\boldsymbol{\nu})$ and $\boldsymbol{D}(\boldsymbol{\nu})$. Mathematically, it implies that the Robust PID control design consists of determining the controller parameters $\boldsymbol{\Gamma}$ in the solution space in $\mathbb{R}^{12}$, considering parametric uncertainties around $\mathcal{M}(\hat{\boldsymbol{\Theta}}^{-})$ in dimensional space $\mathbb{R}^{27}$. This constitutes a challenging problem in view of the dimensions and complex phenomena involved.

IV. METHODOLOGY

Seeking a solution to the problem proposed in Section II, this work proposes the synthesis of PID controllers from the combination of the SLC method and optimal control. The PID tuning is performed by exploring an uncertainty region $\boldsymbol{\Omega}$ around the system initial estimate $\hat{\boldsymbol{\Theta}}^{-}$, using well-spaced samples $\boldsymbol{P}^{\oplus} = [\tilde{\boldsymbol{\Theta}}_1^p, \tilde{\boldsymbol{\Theta}}_2^p, \ldots, \tilde{\boldsymbol{\Theta}}_n^p] \in \boldsymbol{\Omega}$. Subsequently, a single tuning is obtained by minimizing the effects of the uncertainties studied in all the steps defined by the SLC technique. Then, it provides robust PID controllers capable of controlling $\mathcal{M}(\boldsymbol{\Theta})$ for all $\boldsymbol{\Theta} \in \boldsymbol{\Omega}$. It is emphasized that the definition of $\boldsymbol{\Omega}$ is a fundamental step for the method since it establishes the region whose controller should minimize the effects of the uncertainties proposed by the designer.

Mathematically, this new concept can be briefly explained by the following hypothesis: *"if the set $\hat{\boldsymbol{\Theta}}^{-}$ is a rough approximation of $\boldsymbol{\Theta}$, $\boldsymbol{P}^{\oplus} = [\tilde{\boldsymbol{\Theta}}_1^p, \tilde{\boldsymbol{\Theta}}_2^p, \ldots, \tilde{\boldsymbol{\Theta}}_n^p]$ is a set of well spatially benchmark parameters belonging to the uncertainty region $\boldsymbol{\Omega}$ around $\hat{\boldsymbol{\Theta}}^{-}$ and it is possible to design a PID controller $\boldsymbol{u}(t, \boldsymbol{\Gamma}^{\mathcal{C}})$ parameterized by $\boldsymbol{\Gamma}^{+}$, able to control $\mathcal{M}(\boldsymbol{P}^{\oplus})$. Then, the same $\boldsymbol{u}(t, \boldsymbol{\Gamma}^{+})$ will also be able to control $\mathcal{M}(\boldsymbol{\Theta}), \forall \boldsymbol{\Theta} \in \boldsymbol{\Omega}$. Therefore, the designed PID controller parameterized by $\boldsymbol{\Gamma}^{+}$ is considered stable and has robust performance for all $\boldsymbol{\Theta} \in \boldsymbol{\Omega}$, as long as it minimizes: (i) control efforts, (ii) tracking deviations, and (iii) overshoot situations along the chosen tuning scenarios". Minimizing these aspects ensures robust stability, as the optimization process naturally penalizes unstable closed-loop behavior and favors stable tuning, it consequently also tends to the stability of the study region.*

Based on this hypothesis and translating the robust control to an optimal one, the search for tuning the PID controller can be represented by:

$$\mathcal{S}(\mathcal{M}(\boldsymbol{P}^{\oplus}), \Gamma^{-}, \mathcal{X}) = \Gamma^{+}, \tag{21}$$

where $\mathcal{S}(\cdot)$ is the nonlinear optimization algorithm, $\boldsymbol{\Gamma}^{-}$ is the *a priori* PID parameters, $\boldsymbol{\mathcal{X}}$ are the set points defined by SLC technique and $\boldsymbol{\mathcal{M}}(\boldsymbol{P}^{\oplus})$ are the uncertainties needed to find and define $\boldsymbol{u}(t, \boldsymbol{\Gamma}^{+})$.

A. OPTIMIZATION BY INTERIOR-POINTS

The optimization strategy $\mathcal{S}(\cdot)$ was developed based on the Interior Points Algorithm described in [52]. The PID parameters $\boldsymbol{\Gamma}^{+}$ are searched by the controller performance optimization for all uncertainty scenarios proposed by $\boldsymbol{\mathcal{M}}(\boldsymbol{P}^{\oplus})$ using the SLC approach. As previously mentioned, the internal loops are 5 times faster than the external ones. Then, by the SLC definition, the outer loops consider the inner ones as unit gains [53].

To evaluate the performance of the designed control law $\boldsymbol{u}(t, \boldsymbol{\Gamma}^{+})$, an objective function was defined from the following metrics:

1) Minimum control effort ($\boldsymbol{J}_u$): measure the control effort during the experiment described as:

$$\boldsymbol{J}_u = \int_{t_o}^{t_f} [\boldsymbol{\tau}(t, \boldsymbol{\Gamma}^{+})^T \boldsymbol{R} \boldsymbol{\tau}(t, \boldsymbol{\Gamma}^{+})] dt, \tag{22}$$

where $\boldsymbol{\tau} \in [\boldsymbol{\tau}_{min}, \boldsymbol{\tau}_{max}]$ are the signals produced by the actuators, $\boldsymbol{\tau}_{min}$ and $\boldsymbol{\tau}_{max}$ are the minimum and maximum physical actuation system limits, respectively. Furthermore, $\boldsymbol{R}$ is a real symmetric positive definite weighting matrix with constant elements during all the interval simulation time $[t_o, t_f]$.

2) Tracking deviations ($\boldsymbol{J}_e$): compute the system state deviation $\boldsymbol{u}(t)$ from the desired state $\boldsymbol{r}(t)$, defined as:

$$\boldsymbol{J}_e = \int_{t_o}^{t_f} [\boldsymbol{r}(t) - \boldsymbol{x}(t)]^T \boldsymbol{Q} [\boldsymbol{r}(t) - \boldsymbol{x}(t)] dt, \tag{23}$$

where $\boldsymbol{r}(t)$ is the desired state and $\boldsymbol{Q}$ is a real symmetric positive definite weighting matrix with constant elements for the controlled state $\boldsymbol{x}(t)$.

3) Overshoot ($\boldsymbol{\Psi}$): penalize situations where the state $\boldsymbol{x}(t)$ exceed the desired state $\boldsymbol{r}(t)$. The function was defined as:

$$\boldsymbol{\Psi} = \int_{t_o}^{t_f} \alpha(t) |(\boldsymbol{r}(t) - \boldsymbol{x}(t))| dt, \tag{24}$$

where $\alpha(t)$ is defined as:

$$\alpha(t) = \begin{cases} 1, & \forall x_i(t) > r_i(t) \quad \text{and} \quad r_i(t) > 0 \\ 0, & \forall x_i(t) < r_i(t) \quad \text{and} \quad r_i(t) > 0 \\ -1, & \forall x_i(t) < r_i(t) \quad \text{and} \quad r_i(t) < 0 \\ 0, & \forall x_i(t) > r_i(t) \quad \text{and} \quad r_i(t) < 0. \end{cases} \tag{25}$$

Using the metrics described above, the following objective function is proposed to be minimized:

$$\begin{aligned} \underset{\boldsymbol{\Gamma}}{\text{Minimize}} & f(\boldsymbol{\Gamma}) = k_u \boldsymbol{J_u}(\cdot) + k_e \boldsymbol{J_e}(\cdot) + k_\Psi \boldsymbol{\Psi}(\cdot) \\ & \boldsymbol{\Gamma_{min}} \leq \boldsymbol{\Gamma} \leq \boldsymbol{\Gamma_{max}}, \end{aligned} \tag{26}$$

where $\boldsymbol{\Gamma_{min}}$ and $\boldsymbol{\Gamma_{max}}$ are the minimum and maximum limits of $\boldsymbol{\Gamma}$ and k_u, k_e and $k_\Psi \in \mathbb{R}_{\geq 0}$ are constant weightings related to metrics and priorities.

B. METHODOLOGY STEP-BY-STEP

After presenting the details of the optimization technique, it is essential to demonstrate the process, step by step, where every tuned loop was considered independent of each other. Therefore, using the SLC approach within the primary optimization process.

First, every DoF was also manipulated separately. It means that the fast loop (the velocity loop) was tuned before the slow loop (position loop). Then, using this velocity controller, the outer loop is tuned.

Continuing, the first DoF tuned was yawing dynamics. The second one tuned was *Surge* and the last one was *Sway*.

In sequence, all the steps of the proposed tuning method are exposed in the flowchart of Fig. 5:

As previously mentioned, every loop was tuned independently of the other using the Interior Points Algorithm. Yaw dynamics was chosen to be the first for the best ASV nose pointing and energy efficiency (less drag when moving strictly forward). After tuning yawing velocity and consequently its position loop, surge dynamics was settled up for its velocity and position. In the end, sway dynamics was tuned. For this experiment, it was desired that sway displacements should be as low as possible, also for saving energy.

It is important to highlight that after each tuning step, the gains are used in the next one.

V. SIMULATION RESULTS

The simulation results will be presented considering 50 distinct models, generated by normal distribution taking only the non-zero parameters with a maximum of 15% variation. As for the simulation, the 4^{th} order Runge-Kutta numerical method and a sampling interval ΔT of $10ms$ were used. Table 4 reflects the mean (μ) and standard deviation (σ) of the parameters with their *a priori* values $\mathcal{M}(\boldsymbol{\Theta}^-)$:

The weights used in the optimization algorithm were: $k_e = 1.0$, $k_\Psi = 10^3$ and k_u described in Table 5. It is noteworthy that these were defined experimentally to ensure PID tuning that provides stability and robustness to the system.

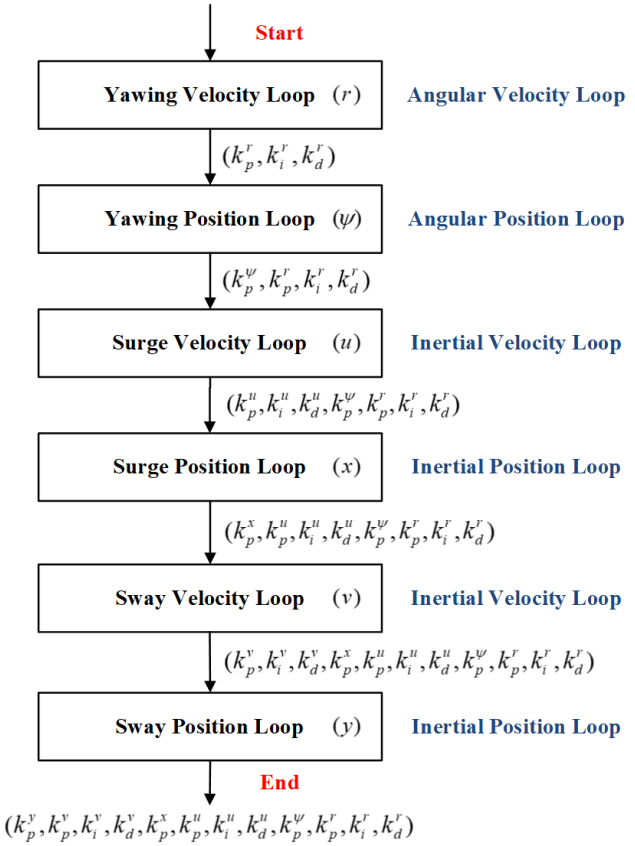

FIGURE 5. Flowchart of the proposed tuning methodology.

TABLE 4. Mean and standard deviation of the parameters for the 50 models compared with their *a priori* values $\mathcal{M}(\boldsymbol{\Theta}^-)$. The other parameters not expressed above are null, as shown in Table 2.

Parameter	Metric	
	μ	σ
$X_{\dot{u}}^- = -17.93$	-17.9782	1.4957
$Y_{\dot{u}}^- = -6.67$	-6.6858	0.5600
$Y_{\dot{v}}^- = -19.93$	-19.93	1.7938
$Y_{\dot{r}}^- = -5.37$	-5.2665	0.4808
$N_{\dot{v}}^- = -5.79$	-5.8318	0.4390
$N_{\dot{r}}^- = -8.49$	-8.7804	0.7168
$X_v^- = -39.93$	-39.7175	3.3444
$X_r^- = -4.77$	-4.8536	0.4264
$N_u^- = -0.93$	-0.9218	0.0783
$N_v^- = -6.89$	-6.9147	0.6069
$X_{\lvert u\rvert u}^- \lvert u\rvert = -7.14$	-7.2659	0.5790
$X_{\lvert u\rvert v}^- \lvert u\rvert = -16.06$	-15.9020	1.1221
$Y_{\lvert v\rvert u}^- \lvert v\rvert = -22.47$	-22.4227	2.0324
$Y_{\lvert v\rvert v}^- \lvert v\rvert = -189.99$	-193.7962	16.7304
$N_{\lvert r\rvert v}^- \lvert v\rvert = -13.30$	-13.1932	1.0702

It is important to highlight that all the 6 controller gains are shown in Table 6 and the evolution of the tuning process (optimization) is displayed in Figs. 6 and 7.

TABLE 5. Weighting of the Minimum Control Effort metric - k_u.

Loop	Velocity	Pose
ψ	0.0750	0.0500
x	0.0350	0.1500
y	0.0100	0.0025

TABLE 6. P-PID controller gains obtained after the proposed optimization.

Variable	P		
x	$k_p^x = 99.01$		
y	$k_p^y = 26.54$		
ψ	$k_p^\psi = 20.54$		
	P	**I**	**D**
u	$k_p^u = 97.81$	$k_i^u = 21.35$	$k_d^u = 2.54$
v	$k_p^v = 136.46$	$k_i^v = 11.92$	$k_d^v = 19.60$
r	$k_p^r = 31.26$	$k_i^r = 28.34$	$k_d^r = 15.18$

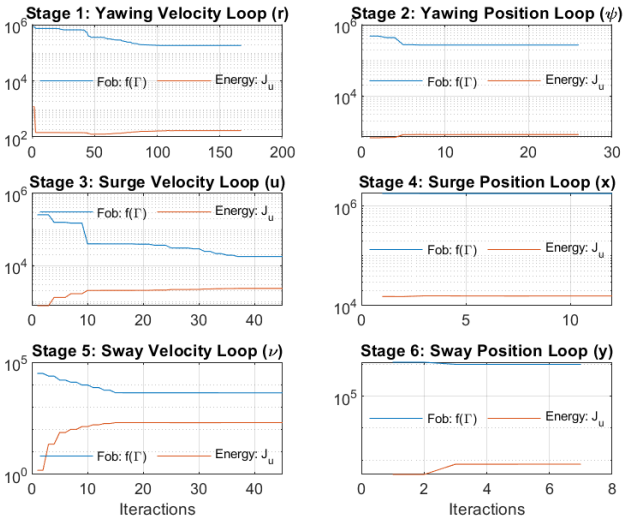

FIGURE 6. Objective function $f(\Gamma)$ evolution and comparison with the Control Energy effort ($\mathcal{J}_u$) in the 6 stages of the methodology, Scenario 1.

Figures 6 and 7 illustrate the optimization process behavior in the 6 stages of tuning the controllers, which result in Table 6. Specifically, in Fig. 6, the evolution of the objective function and also the metric referring to $\mathcal{J}_u$ are observed. In this scenario, the behavior of the minimization of $f(\Gamma)$ is clearly perceived, while the controller's effort in providing the necessary actions is also considered. Figure 7 shows the evolution of each tuning stage that provides feasible values, according to the expected and presented data in Table 6.

To test the proposed controller tuning robustness, 3 different scenarios will be performed, which are:

- Scenario 1 (Subsection V-A): The starting point inside the desired path with ASV's parameters within the %15 variation;

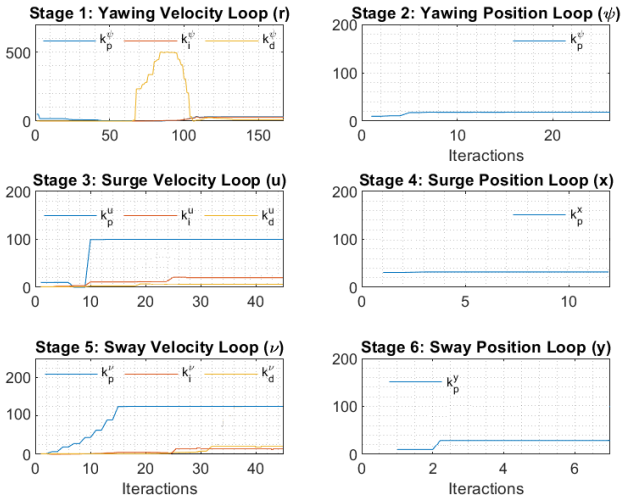

FIGURE 7. Results of the controller tuning process in the 6 stages of the methodology, Scenario 1.

- Scenario 2 (Subsection V-B): The starting point outside the desired path with ASV's parameters within the %15 variation;
- Scenario 3 (Subsection V-C): The starting point inside the desired path with ASV's parameters beyond the %15 variation (critical variation): $|\pm 20\%|$, $|\pm 30\%|$ and $|\pm 40\%|$.

The chosen path has a square format, considering that the ASV needs to go through it without breaking when the turn is reached. The reason for this choice is to test the controller trackability when the setpoint is unpredictably changed.

The Integral of the Squared Error (ISE) was considered for the scenario quantitative analysis, in which the definition is the error between the desired and the ASV state variables. It is defined by:

$$\boldsymbol{ISE} = \sum_{i=0}^{i=N} (\boldsymbol{x}^d(i) - \boldsymbol{x}(i))^2, \tag{27}$$

where N is the total number of iterations, $\boldsymbol{x}^d$ is the desired setpoint vector for the 6 controlled variables, represented by $[\boldsymbol{x}^d, \boldsymbol{y}^d, \boldsymbol{\psi}^d, \boldsymbol{u}^d, \boldsymbol{v}^d, \boldsymbol{r}^d]$. Finally, $\boldsymbol{x}$ represents the data vector from the simulation results $[\boldsymbol{x}, \boldsymbol{y}, \boldsymbol{\psi}, \boldsymbol{u}, \boldsymbol{v}, \boldsymbol{r}]$.

It is also important to mention that all simulation tests used an Intel(R) Core (TM) i7-2600 device with 3.4GHz 8GB of RAM and Windows operational system 7 with 64 Bits. It is important to highlight that the computational capacity of the entire embedded control board was emulated on this i7-2600 computer, to perform the ASV for future experimental tests better.

A. SCENARIO 1

This scenario is created to illustrate a path where the ASV starts inside the desired path also with its modeled parameters within the 15% considered variation.

TABLE 7. Desired WPs for the performed path shown in Fig. 8, Scenario 1.

WP Number	X $[m]$	Y $[m]$
1	-10	10
2	0	20
3	10	10
4	0	0

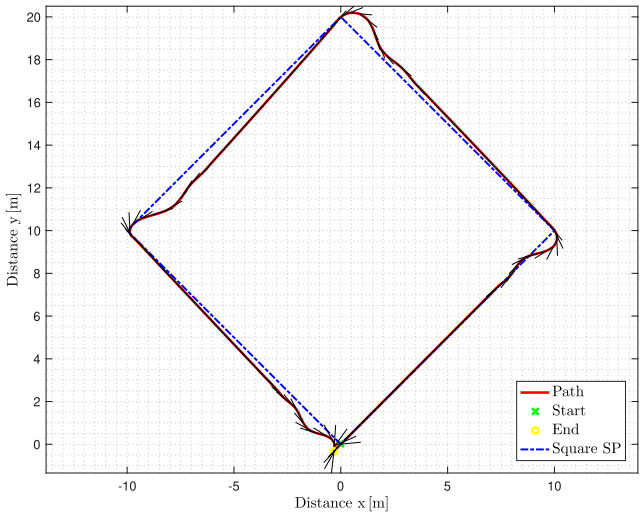

FIGURE 8. Simulation results for the desired and performed path considering the *a priori* model, Scenario 1.

Taking the *a priori* model into account, i.e., the model with the pure and estimated values is shown in work [42].

The setpoints x^d and y^d are always looking to the next WP. The ψ^d setpoint is obtained through the angle between x^d and y^d. Then, the ASV will not follow the dashed blue line, i.e., it will always go straight to the next WP. It is possible to highlight that a 1 meter WP radius was settled, which means when the ASV is inside of a 1 meter radius location to the desired WP, the WP number is changed for the next one and the ASV will start tracking the next location.

Figure 8 presents the controlled variables x, y, ψ, u, v and r for the desired path presented in Fig. 9 for Table 7.

The 6 controlled variables (red lines) showed that the WP corners were quickly reached, which means that the proposed P-PID controlled the ASV satisfactorily.

This is also clear by analyzing the 2 controlled variables: u, and ψ, for each WP in Table 8. Note that control loops provided stabilization time minor than $T_s^u \leqq 1.75s$, $T_s^\psi \leqq 3.42s$, and overshoots (%) that are $UP^u = 0\%$ and do not exceed $UP^\psi \leqq 22.5\%$.

Furthermore, it is necessary to highlight the system saturation in the r controlled variable (yawing dynamics), explained due to the ASV's length and z inertial moment. Regarding sway dynamics, it is possible to see that its desired velocity was always $0m/s$, i.e., the ASV is not desired to perform sideslip. Therefore, these indices presented reasonable results for the controller design requirements.

Now, taking the simulation of the 50 models with the 6 tuned controllers, Table 9 depicts the mean (μ) and standard deviation (σ) values of the ISE for the variables x, y,ψ,u, v and r:

TABLE 8. Performance indices for the controlled variables shown in Fig. 9, Scenario 1.

WP Number	T_s^u	T_s^ψ / UP^ψ
1	$1.16s$	$3.42s/22.5\%$
2	$1.57s$	$2.67s/20.7\%$
3	$1.75s$	$2.56s/21.1\%$
4	$1.14s$	$3.05s/20.1\%$

TABLE 9. Mean (μ) and standard deviation (σ) values of the ISE index for the 6 controlled variables, Scenario 1.

Variable	Metric	
	μ	σ
x	1458.2	13.7
y	1574.7	24.0
ψ	404660.1	1075.7
u	7.2	0.5
v	0.5	0.5
r	162849.0	26456.5

Analyzing the data from the table above, it is possible to see higher numbers for yaw position and velocity (ψ and r, respectively), which is explained by the difficulty of sway maneuverability. It is known from Table 1 that mass and z inertial moments are quite expressive for ASVs with the embedded actuator's requirements. As consequence, yaw angular velocity is naturally saturated.

To finish the presentation of the simulation results, Fig. 10 illustrates the information about the following dataset characteristics: location, dispersion, asymmetry, tail length, and outliers. This graph was obtained considering the Root-Mean Square Error (RMSE) with tuned velocity controllers for Scenario 1 (Fig. 8), taking the 50 distinct models into account (Table 4).

Table 4 shows that the linear velocities obtained quite reasonable mean values and RMSE distribution. The compact distribution demonstrates the controller's robustness, capable of dealing with the proposed uncertainties for the 50 models in the range $|\pm 15\%|$. In addition, average values around 0.44 m/s for Surge and 0.11 m/s for Sway also demonstrate robust results, knowing that the proposed scenario provided conditions of considerable parameter uncertainties. Under these conditions, the errors are within an acceptable range according to the work [42]. As for the angular velocity (yaw speed), an RMSE around 15.5 deg/s was obtained, also acceptable, given the ASV inertial characteristics and the large steering conditions in Scenario 1.

B. SCENARIO 2

The second scenario illustrates a situation where the ASV starts far from the desired path with its modeled parameters within the %15 considered variation.

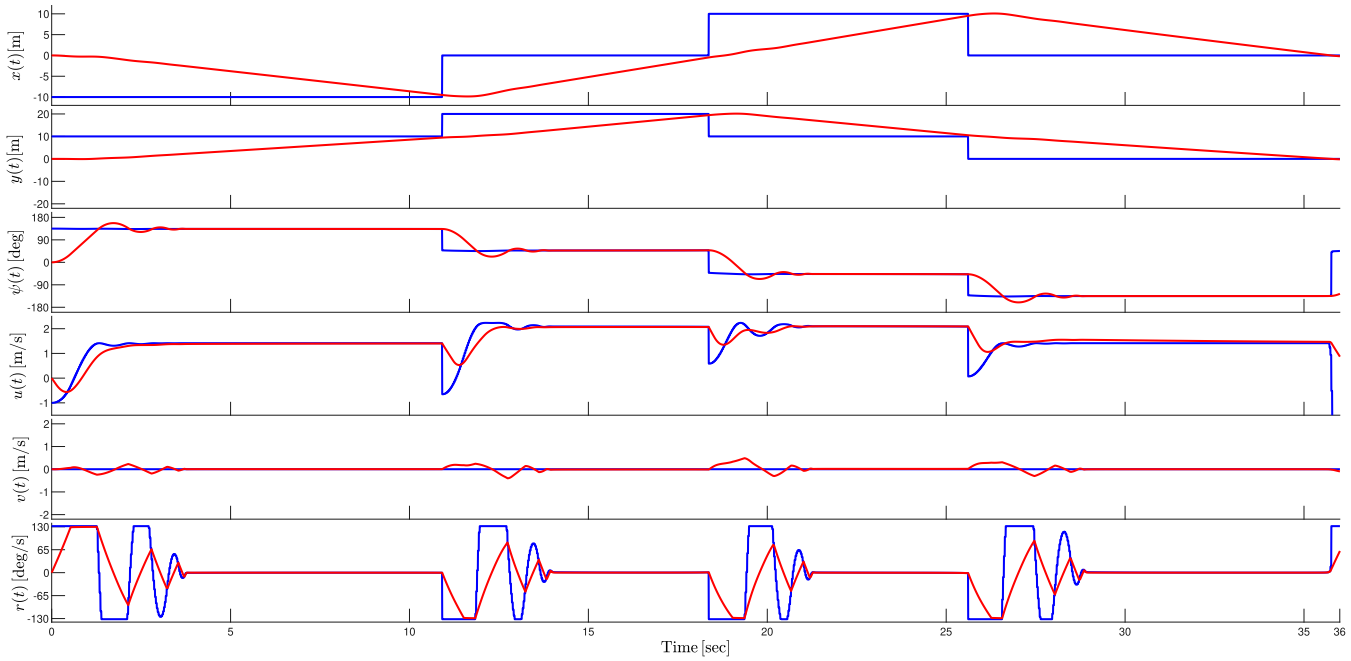

FIGURE 9. Simulation results for the 6 controlled variables of Scenario 1 considering the *a priori* model, Scenario 1.

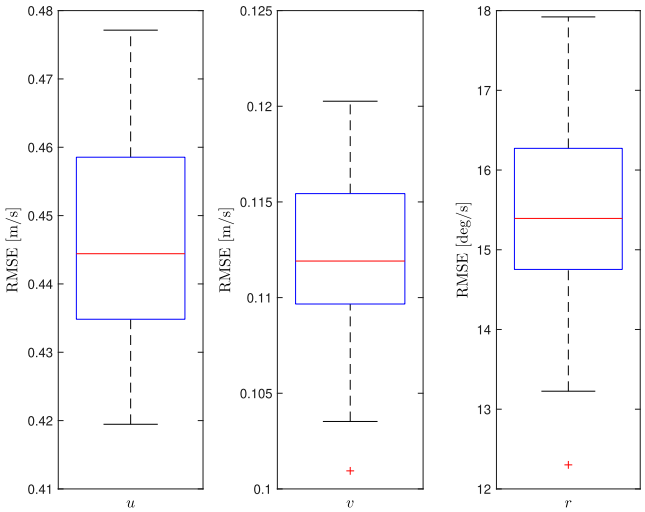

FIGURE 10. Dispersion graph for the RMSE of 3 velocity controlled state variables for 50 distinct models for Scenario 1.

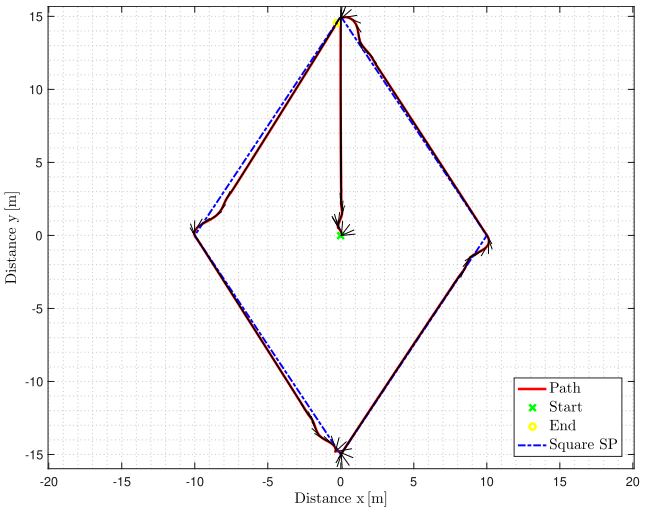

FIGURE 11. Simulation results for the desired and performed path considering the *a priori* model, Scenario 2.

TABLE 10. Desired WPs for the performed path shown in Fig. 12, Scenario 2.

WP Number	X $[m]$	Y $[m]$
1	0	15
2	10	0
3	0	-15
4	-10	0

Figure 11 presents the controlled variables for the path presented in Fig. 12 for Table 10.

At the beginning of the simulation it is possible to check the ASV performing movements to go directly to the first WP, which is reached in around 16s.

Furthermore, observing the control loop behaviors through Fig. 12, it is noted that the controller provided satisfactory trackability, even in the difficult condition of abrupt changes provided by the corners. According to the results, the ASV obtained dynamics with $T_s^u \leqq 2.14s$, $T_s^\psi \leqq 3.30s$, and overshoots (%) that are $UP^u = 0\%$ and do not exceed $UP^\psi \leqq 25.2\%$.

C. SCENARIO 3

Here the path of Scenario 1 with 3 variations of parameters out of the permitted range: 20, 30, and 40% beyond the maximum range permitted in the tuning step is considered.

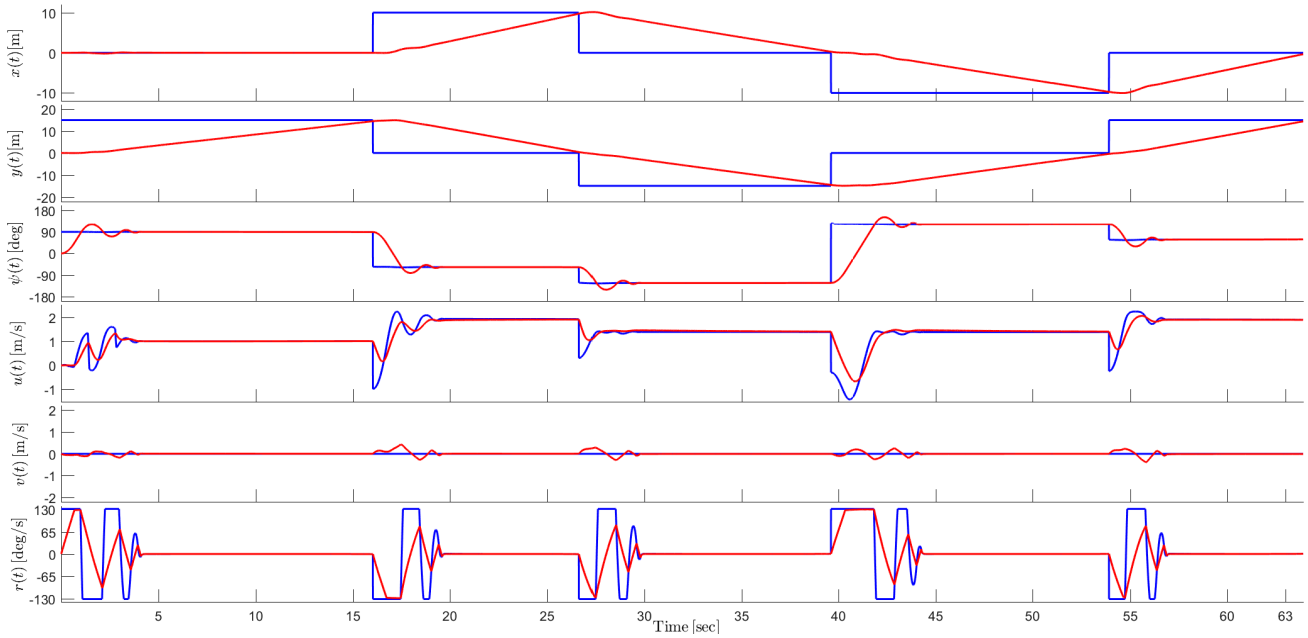

FIGURE 12. Simulation results for the 6 controlled variables of Scenario 2 considering the *a priori* model, Scenario 2.

TABLE 11. Parameters and their variations for Scenario 3.

$\mathcal{M}(\hat{\Theta}^+)$	$X_{\dot{u}}$	$Y_{\dot{v}}$	$N_{\dot{r}}$
μ	-17.9782	-19.9300	-8.7804
$\mid \pm 20\% \mid$	-21.5738	-15.9440	-10.5365
$\mid \pm 30\% \mid$	-12.5847	-25.9090	-7.0243
$\mid \pm 40\% \mid$	-25.1695	-27.9020	-12.2926

The main idea for this choice is to prove the proposed methodology robustness.

The parameters and their values are shown in Table 11. They were chosen due to the difficulty to get them from the real prototype measurements [13]. Also, they were compared with their mean values, from Table 4:

Figure 13 shows the paths performed for the 4 different models with the same P-PID controller previously tuned:

The above figure brings out the possibility to analyze the proposed methodology for tuning the ASV controllers (gains shown in Table 6). The red line represents the ASV in simulations with their parameters within the considered range in the tuning controller stage. The black, green and cyan lines represent the ASV with parameter out of the permitted range, $\mid \pm 20\% \mid$, $\mid \pm 30\% \mid$ and $\mid \pm 40\% \mid$, respectively. Then, the controller's capability to deal with large variations of the 3 most sensible parameters is visible.

Some metrics are shown in Table 12 for quantitative analysis of their controlled responses:

The above table shows that the control requirements of the models extrapolating the parameter range were considerably depreciated compared to the model with the permitted parameter ranges in the tuning procedure. These indices were

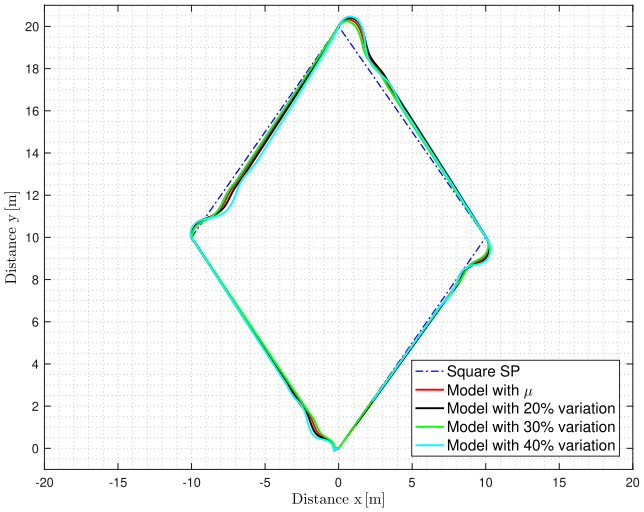

FIGURE 13. Simulation results for the performed path, Scenario 3.

highlighted in red. Even though, the path was performed with no reached boundary limits, demonstrating robustness and reliability.

Still, in Table 12, it is concluded that the methodology is capable of minimizing the effects of parametric uncertainties, even in adverse situations such as the scenarios of $\mid \pm 30\% \mid$ and $\mid \pm 40\% \mid$ variations. The transient indices results also demonstrate that the designed controller provided stability in all uncertainty scenarios. Therefore, it is valid to state that the hypothesis raised in Section IV provides control laws with stability and robust performance to small regions of

TABLE 12. Performance indices for the controlled variables shown in Fig. 13 for every WP, Scenario 3.

		WP Number			
$\mathcal{M}(\hat{\Theta}^{+})$	Metric	1	2	3	4
μ	T_s^u	1.16s	1.57s	1.75s	1.14s
	T_s^ψ	3.42s	2.67s	2.56s	3.05s
	UP^ψ	22.5%	20.7%	21.1%	20.1%
$\lvert \pm 20\% \rvert$	T_s^u	4.12s	4.23s	3.33s	4.49s
	T_s^ψ	4.03s	3.27s	3.48s	3.63s
	UP^ψ	23.8%	27.8%	24.19%	24.3%
$\lvert \pm 30\% \rvert$	T_s^u	4.2s	3.59s	3.33s	3.94s
	T_s^ψ	4.21s	3.05s	3.1s	2.82s
	UP^ψ	27.4%	28.8%	25.1%	26.7%
$\lvert \pm 40\% \rvert$	T_s^u	**4.81s**	**4.52s**	**4.51s**	**4.3s**
	T_s^ψ	**4.39s**	**4.68s**	**4.30s**	**4.62s**
	UP^ψ	**29.4%**	**39.2%**	**33.6%**	**37.4%**

uncertainty, defined around *a priori* estimations of the desired system.

VI. CONCLUSION

This work has proposed a new methodology of controller tuning for an ASV prototype considering uncertainties in the 50 distinct models.

The new methodology for controller tuning was formulated as a sequence of multiple optimization procedures, always considering 50 different models with at most 15% of parameter variations. Every loop was tuned independently of the other using the Interior Points Algorithm. The first tuned controller was yaw dynamics, which directly deals with the ASV steering. After tuning yawing velocity and consequently its position loop, surge dynamics was settled up for its velocity and position. In the end, sway dynamics was tuned. Furthermore, after each tuning stage, the gains were used in the next loop, consecutively, until getting all 6 controller gains, as summarized in the flowchart of Fig. 5.

Concerning the control loop assessment, it is possible to remark the presence of overshoots less than 22.5% for yaw position dynamics and settling times less than 3.42 and 1.75*s* for surge velocity and yaw position dynamics, respectively. These values were within the control requirements in the tuning stage.

Even though the used *a priori* parameter model was from the work [42], and validated with open-field experiments, the proposition of this work shows the importance of the existence of robust controllers, not based only on one model, but tuned considering uncertainties in the model's parameters.

The results have demonstrated that the proposed methodology has robustness, applicability, and reliability, where the 6 P-PID controllers performed the setpoints for many distinct models with uncertainty parameters, even when considerable variations were tested out of the permitted range in the controller tuning step.

Finally, as future work, the proposed controller tuning will be performed in open-field tests on the developed prototype.

REFERENCES

[1] Z. Liu, Y. Zhang, X. Yu, and C. Yuan, "Unmanned surface vehicles: An overview of developments and challenges," *Annu. Rev. Control*, vol. 41, pp. 71–93, Jan. 2016.
[2] V. Jorge, R. Granada, R. Maidana, D. Jurak, G. Heck, A. Negreiros, D. Dos Santos, L. Gonçalves, and A. Amory, "A survey on unmanned surface vehicles for disaster robotics: Main challenges and directions," *Sensors*, vol. 19, no. 3, p. 702, Feb. 2019.
[3] Z. Peng, J. Wang, D. Wang, and Q.-L. Han, "An overview of recent advances in coordinated control of multiple autonomous surface vehicles," *IEEE Trans. Ind. Informat.*, vol. 17, no. 2, pp. 732–745, Jun. 2021.
[4] P. Mahacek, "Dynamic analysis of a SWATH vessel," *MBARI Internship Rep.*, pp. 1–13, 2005. [Online]. Available: https://www.semanticscholar.org/paper/Dynamic-Analysis-of-a-SWATH-Vessel-Mahacek/fd3af3ac4e7e08d6ffebe5b0f43aa1568510f8a2#citing-papers
[5] J. Curcio, J. Leonard, and A. Patrikalakis, "SCOUT—A low cost autonomous surface platform for research in cooperative autonomy," in *Proc. OCEANS MTS/IEEE*, Sep. 2005, pp. 725–729.
[6] H. Ferreira, R. Martins, E. Marques, J. Pinto, A. Martins, J. Almeida, J. Sousa, and E. P. Silva, "SWORDFISH: An autonomous surface vehicle for network centric operations," in *Proc. OCEANS Eur.*, Jun. 2007, pp. 1–6.
[7] E. Beck, W. Kirkwood, D. Caress, T. Berk, P. Mahacek, K. Brashem, J. Acain, V. Reddy, C. Kitts, J. Skutnik, and G. Wheat, "SeaWASP: A small waterplane area twin hull autonomous platform for shallow water mapping," *Mar. Technol. Soc. J.*, vol. 43, no. 1, pp. 6–12, Mar. 2009.
[8] U. K. Verfuss, A. S. Aniceto, D. V. Harris, D. Gillespie, S. Fielding, G. Jiménez, P. Johnston, R. R. Sinclair, A. Sivertsen, S. A. Solbø, R. Storvold, M. Biuw, and R. Wyatt, "A review of unmanned vehicles for the detection and monitoring of marine fauna," *Mar. Pollut. Bull.*, vol. 140, pp. 17–29, Mar. 2019.
[9] T. I. Fossen, *Marine Control Systems: Guidance. Navigation, and Control of Ships, Rigs and underwater Vehicles*. Trondheim, Norway: Typir Trykkeri, 2002.
[10] N. Wang, S. Lv, M. J. Er, and W.-H. Chen, "Fast and accurate trajectory tracking control of an autonomous surface vehicle with unmodeled dynamics and disturbances," *IEEE Trans. Intell. Veh.*, vol. 1, no. 3, pp. 230–243, Sep. 2016.
[11] A. Odetti, M. Altosole, G. Bruzzone, M. Viviani, and M. Caccia, "A new concept of highly modular ASV for extremely shallow water applications," *IFAC-PapersOnLine*, vol. 52, no. 21, pp. 181–186, 2019.
[12] Y. Peng, Y. Yang, J. Cui, X. Li, H. Pu, J. Gu, S. Xie, and J. Luo, "Development of the USV 'JingHai-I' and sea trials in the southern yellow sea," *Ocean Eng.*, vol. 131, pp. 186–196, Feb. 2017.
[13] B. A. Regina, L. M. Honório, A. A. N. Pancoti, M. F. Silva, M. F. Santos, V. M. L. Lopes, A. F. S. Neto, and L. G. F. Westin, "Hull and aerial holonomic propulsion system design for optimal underwater sensor positioning in autonomous surface vessels," *Sensors*, vol. 21, no. 2, p. 571, Jan. 2021.
[14] K. Zhou and J. C. Doyle, *Essentials Robust Control*, vol. 104. Upper Saddle River, NJ, USA: Prentice-Hall, 1998.
[15] R. K. Yedavalli, *Robust Control of Uncertain Dynamic Systems*. New York, NY, USA: Springer, 2016.
[16] L. Ding, A. Johansson, and T. Gustafsson, "Application of reduced models for robust control and state estimation of a distributed parameter system," *J. Process Control*, vol. 19, no. 3, pp. 539–549, Mar. 2009.
[17] M. F. da Silva, L. M. de Mello Honório, M. F. dos Santos, A. F. dos Santos Neto, N. A. Cruz, A. C. C. Matos, and L. G. F. Westin, "Project and control allocation of a 3 DoF autonomous surface vessel with aerial azimuth propulsion system," *IEEE Access*, vol. 9, pp. 5212–5227, 2021.
[18] C.-Z. Pan, X.-Z. Lai, S. X. Yang, and M. Wu, "An efficient neural network approach to tracking control of an autonomous surface vehicle with unknown dynamics," *Exp. Syst. Appl.*, vol. 40, no. 5, pp. 1629–1635, Apr. 2013.
[19] M. Caccia, M. Bibuli, R. Bono, and G. Bruzzone, "Basic navigation, guidance and control of an unmanned surface vehicle," *Auto. Robots*, vol. 25, no. 4, pp. 349–365, Nov. 2008.
[20] J. Qi, Y. Peng, H. Wang, and J. Han, "Design and implement of a trimaran unmanned surface vehicle system," in *Proc. Int. Conf. Inf. Acquisition*, Jul. 2007, pp. 361–365.
[21] J.-H. Park, H.-W. Shim, B.-H. Jun, S.-M. Kim, P.-M. Lee, and Y.-K. Lim, "A model estimation and multi-variable control of an unmanned surface vehicle with two fixed thrusters," in *Proc. OCEANS IEEE SYDNEY*, May 2010, pp. 1–5.

[22] K. J. Åström and T. Hägglund, "PID controllers: Theory," *Des., Tuning*, vol. 2, pp. 59–120, Jun. 1995.
[23] M. N. Azzeri, F. A. Adnan, and M. Z. Md. Zain, "Review of course keeping control system for unmanned surface vehicle," *Jurnal Teknologi*, vol. 74, no. 5, pp. 1–10, May 2015.
[24] D. D. A. Fernandes, A. J. Sørensen, K. Y. Pettersen, and D. C. Donha, "Output feedback motion control system for observation class ROVs based on a high-gain state observer: Theoretical and experimental results," *Control Eng. Pract.*, vol. 39, pp. 90–102, Jun. 2015.
[25] C. J. Boss and V. Srivastava, "A high-gain observer approach to robust trajectory estimation and tracking for a multi-rotor UAV," 2021, *arXiv:2103.13429*.
[26] J. Lu, S. Yu, G. Zhu, Q. Zhang, C. Chen, and J. Zhang, "Robust adaptive tracking control of UMSVs under input saturation: A single-parameter learning approach," *Ocean Eng.*, vol. 234, Aug. 2021, Art. no. 108791.
[27] S. Kragelund, V. Dobrokhodov, A. Monarrez, M. Hurban, and C. Khol, "Adaptive speed control for autonomous surface vessels," in *Proc. OCEANS*, San Diego, CA, USA, Sep. 2013, pp. 1–10.
[28] A. S. K. Annamalai, R. Sutton, C. Yang, P. Culverhouse, and S. Sharma, "Robust adaptive control of an uninhabited surface vehicle," *J. Intell. Robot. Syst.*, vol. 78, no. 2, pp. 319–338, 2015.
[29] A. Haseltalab and R. R. Negenborn, "Adaptive control for autonomous ships with uncertain model and unknown propeller dynamics," *Control Eng. Pract.*, vol. 91, Oct. 2019, Art. no. 104116.
[30] Z. Sun, G. Zhang, Y. Lu, and W. Zhang, "Leader-follower formation control of underactuated surface vehicles based on sliding mode control and parameter estimation," *ISA Trans.*, vol. 72, pp. 15–24, Jan. 2018.
[31] H. Nurhadi, E. Apriliani, T. Herlambang, and D. Adzkiya, "Sliding mode control design for autonomous surface vehicle motion under the influence of environmental factor," *Int. J. Electr. Comput. Eng. (IJECE)*, vol. 10, no. 5, p. 4789, Oct. 2020.
[32] Y. Yan, S. Yu, and C. Sun, "Event-triggered sliding mode tracking control of autonomous surface vehicles," *J. Franklin Inst.*, vol. 358, no. 8, pp. 4393–4409, May 2021.
[33] E. Kamal, A. Aitouche, R. Ghorbani, and M. Bayart, "Robust nonlinear control of wind energy conversion systems," *Int. J. Electr. Power Energy Syst.*, vol. 44, no. 1, pp. 202–209, Jan. 2013.
[34] K. Shojaei, "Neural adaptive robust control of underactuated marine surface vehicles with input saturation," *Appl. Ocean Res.*, vol. 53, pp. 267–278, Oct. 2015.
[35] L. G. García-Valdovinos, T. Salgado-Jiménez, M. Bandala-Sánchez, L. Nava-Balanzar, R. Hernández-Alvarado, and J. A. Cruz-Ledesma, "Modelling, design and robust control of a remotely operated underwater vehicle," *Int. J. Adv. Robotic Syst.*, vol. 11, no. 1, p. 1, Jan. 2014.
[36] S.-S. Hu and J.-Y. Juang, "Robust nonlinear ship course-keeping control under the influence of high wind and large wave disturbances," in *Proc. 8th Asian Control Conf. (ASCC)*, 2011, pp. 393–398.
[37] E. Chnib, O. Sename, F. Ferrante, E. R. Canales, and J. C. Luque, "Decoupled control of a twin hull-based unmanned surface vehicle using a linear parameter varying approach," in *Proc. 10th Int. Conf. Mechatronics Control Eng.*, 2021, pp. 87–100.
[38] Q. Yao, Y. Tian, Q. Wang, and S. Wang, "Control strategies on path tracking for autonomous vehicle: State of the art and future challenges," *IEEE Access*, vol. 8, pp. 161211–161222, 2020.
[39] P. H. Petkov, J. Kralev, and T. Slavov, "Design and implementation of robust control laws," in *Proc. 29th Eur. Conf. Model. Simul. (ECMS)*, May 2015, pp. 6–18.
[40] P. Dini and S. Saponara, "Processor-in-the-loop validation of a gradient descent-based model predictive control for assisted driving and obstacles avoidance applications," *IEEE Access*, vol. 10, pp. 67958–67975, 2022.
[41] N. Guo, X. Zhang, Y. Zou, B. Lenzo, and T. Zhang, "A computationally efficient path-following control strategy of autonomous electric vehicles with yaw motion stabilization," *IEEE Trans. Transport. Electrific.*, vol. 6, no. 2, pp. 728–739, Jun. 2020.
[42] A. F. D. S. Neto, L. De Mello Honório, M. F. Da Silva, I. C. Da Silva Junior, and L. G. F. Westin, "Development of optimal parameter estimation methodologies applied to a 3DOF autonomous surface vessel," *IEEE Access*, vol. 9, pp. 50035–50049, 2021.
[43] T. I. Fossen, *Guidance and Control of Ocean Vehicles*. New York, NY, USA: Wiley, 1994.
[44] T. I. Fossen, *Handbook of Marine Craft Hydrodynamics and Motion Control*. Hoboken, NJ, USA: Wiley, 2011.
[45] M. F. Santos, L. M. Honório, A. P. G. M. Moreira, P. A. N. Garcia, M. F. Silva, and V. F. Vidal, "Analysis of a fast control allocation approach for nonlinear over-actuated systems," *ISA Trans.*, vol. 126, pp. 545–561, Jul. 2022.
[46] M. F. Santos, L. M. Honório, A. P. G. M. Moreira, M. F. Silva, and V. F. Vidal, "Fast real-time control allocation applied to over-actuated quadrotor tilt-rotor," *J. Intell. Robotic Syst.*, vol. 102, no. 3, pp. 1–20, Jul. 2021.
[47] P. Burggräf, A. R. Pérez Martínez, H. Roth, and J. Wagner, "Quadrotors in factory applications: Design and implementation of the quadrotor's P-PID cascade control system," *Social Netw. Appl. Sci.*, vol. 1, no. 7, p. 722, Jul. 2019.
[48] A. C. Z. D. Souza, L. M. Honório, G. L. Torres, and G. Lambert-Torres, "Increasing the loadability of power systems through optimal-local-control actions," *IEEE Trans. Power Syst.*, vol. 19, no. 1, pp. 188–194, Feb. 2004.
[49] J. E. Dennis and R. B. Schnabel, *Numerical Methods for Unconstrained Optimization and Nonlinear Equations*, vol. 16. Philadelphia, PA, USA: SIAM, 1996.
[50] E. R. Herrero and F. J. V. González, "Two-step identification of non-linear manoeuvring models of marine vessels," *Ocean Eng.*, vol. 53, pp. 72–82, Oct. 2012.
[51] J. Cui and H. Sun, "Fixed-time trajectory tracking control of autonomous surface vehicle with model uncertainties and disturbances," *Complexity*, vol. 2020, pp. 1–10, Oct. 2020.
[52] R. H. Byrd, J. C. Gilbert, and J. Nocedal, "A trust region method based on interior point techniques for nonlinear programming," *Math. Program.*, vol. 89, no. 1, pp. 149–185, Nov. 2000.
[53] R. W. Beard and T. W. McLain, *Small Unmanned Aircraft: Theory and Practice*. Princeton, NJ, USA: Princeton Univ. Press, 2012.

MURILLO FERREIRA DOS SANTOS received the B.Eng. degree in control and automation engineering from CEFET-MG, in 2012, and the M.Eng. and D.Eng. degrees in electrical engineering from the Federal University of Juiz de Fora, in 2014 and 2019, respectively. He is involved in research and development projects (R&D) in robotics with an emphasis on unmanned autonomous aerial vehicles (UAVs) for more than nine years. He is currently an Associate Professor with Centro Federal de Educação Tecnológica de Minas Gerais (CEFET-MG), where he teaches robotics, process control, and automation. His research interests include nonlinear control theory, aerial and aquatic robotics, automation, and control allocation techniques.

ACCACIO FERREIRA DOS SANTOS NETO received the B.Eng. degree in electrical engineering and the M.Eng. degree in computational modeling from the Federal University of Juiz de Fora (UFJF), in 2010 and 2013, respectively, where he is currently pursuing the D.Eng. degree in electrical engineering. He is currently an Assistant Professor with the Centro Federal de Educação Tecnológica de Minas Gerais (CEFET-MG). His current research interests include process control, system identification, and modeling and control of surface marine vehicle.

LEONARDO DE MELLO HONÓRIO received the B.Eng. degree from the Federal University of Juiz de Fora (UFJF), in 1993, and the M.Sc. and D.Sc. degrees from UNIFEI, Brazil, in 1999 and 2002, respectively, all in electrical engineering. He was a Visiting Researcher at the University of California, Irvine, in 2006, and Porto University, in 2012. He is currently a Full Professor with UFJF. His current research interests include evolutionary algorithms, probabilistic methods, electrical power systems, robotics, autonomous vehicles, fuzzy logic, pattern recognition, and optimization.

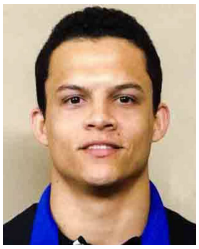

MATHAUS FERREIRA DA SILVA received the B.Eng. degree in control and automation engineering from Centro Federal de Educação Tecnológica de Minas Gerais (CEFET-MG), in 2015, and the M.Eng. and D.Eng. degrees in electrical engineering from Federal University of Juiz de Fora (UFJF), in 2017 and 2021, respectively. He has been involved in research and development projects (R&D) in robotics with an emphasis on unmanned autonomous aerial vehicles and autonomous surface vehicles (ASVs) for more than seven years. His main research interests include unmanned aerial vehicles (UAVs), autonomous surface vehicles (ASVs), stochastic methods, navigation, control, automation, and optimization.

PAOLO MERCORELLI (Member, IEEE) received the master's degree in electronic engineering from the University of Florence, Florence, Italy, in 1992, and the Ph.D. degree in systems engineering from the University of Bologna, Bologna, Italy, in 1998. In 1997, he was a Visiting Researcher for one year at the Department of Mechanical and Environmental Engineering, University of California, Santa Barbara. From 1998 to 2001, he held a postdoctoral position at Asea Brown Boveri, Heidelberg, Germany. From 2002 to 2005, he was a Senior Researcher and the Leader of the Control Group, the Institute of Automation and Informatics, Wernigerode, Germany. From 2005 to 2011, he was an Associate Professor of process informatics at the Ostfalia University of Applied Sciences, Wolfsburg, Germany. Since 2012, he has been a Full Professor (Chair) of control and drive systems with the Institute for Production Technology and Systems (IPTS), Leuphana University of Lueneburg, Lueneburg, Germany. His current research interests include mechatronics, automatic control, and signal processing.